

Bulk Flow Regimes and Fractional Flow in 2D Porous Media by Numerical Simulations

HENNING ARENDT KNUDSEN^{1,2} (arendt@phys.ntnu.no),
 EYVIND AKER^{3,4,5} (eaker@fys.uio.no) and ALEX HANSEN^{1,2}
 (alex.hansen@phys.ntnu.no)

¹*Department of Physics, Norwegian University of Science and Technology, NTNU, N-7491 Trondheim, Norway*

²*Nordita, Blegdamsvej 17, DK-2100 Copenhagen, Denmark*

³*Department of Physics, University of Oslo, N-0316 Oslo, Norway*

⁴*Niels Bohr Institute, Blegdamsvej 17, DK-2100 Copenhagen, Denmark*

⁵*Schlumberger Geco-Prakla, Solbråvn 23, N-1370 Asker, Norway*

Abstract. We investigate a two-dimensional network simulator that model the dynamics of two-phase immiscible bulk flow where film flow can be neglected. We present a method for simulating the detailed dynamical process where the two phases are allowed to break up into bubbles and bubbles are allowed to merge together. The notions of drainage and imbibition are not adequate to describe this process since there is no clear front between the fluids. In fact the simulator is constructed so that one can study the behaviour of the system far from inlets and outlets where the two fluids have been mixed together so much that all initial fronts have broken up. The simulator gives the fractional flow as a function the saturation of each of the fluids. For the case of two fluids with equal viscosity, we classify flow regimes that are parametrized by the capillary number.

Keywords: network modelling, immiscible, two-phase flow, capillary and viscous forces, fractional flow, bulk flow, flow regimes

1. Introduction

Two-phase displacements have been studied by experimental work (Chen and Wilkinson, 1985; Måløy et al., 1985; Lenormand et al., 1988), numerical simulations (Koplik and Lasseter, 1985; Lenormand et al., 1988; Blunt and King, 1990), statistical models (Witten and Sander, 1981; Wilkinson and Willemsen, 1983; Paterson, 1984) and differential equations (Binning and Celia, 1998) during the past decades. Real-world motivations for work in this field are oil-recovery and hydrology.



© 2020 Kluwer Academic Publishers. Printed in the Netherlands.

The complex nature of the problem makes it worthwhile to approach the problem in many ways.

In this paper we present a simulator that provides fractional flow curves as a function of saturation in a steady-state situation without boundaries. Much work in the field of fractional flow has been done by means of solving differential equations, see for example Binning and Celia (1998) and references therein. There has also been numerical work, see Rothman (1990). The classical work in this field is that of Buckley and Leverett (1942). See also Dullien (1992) for a broader presentation.

Since we are dealing with a closed system without boundaries and no clear front, the notions of drainage and imbibition are not adequate to describe the process in this model system. We have therefore made a new classification of the flow regimes; viscous force-dominated regime, viscous and capillary interaction regime, and capillary force-dominated regime. We refer to them as bulk flow regimes, and they are characterized by different behaviour of the fractional flow curves as a function of saturation. The two first are also found to be history independent regimes, whereas the third regime shows history dependence. This paper is primarily concerned with the history independent regimes.

The simulator is based on a simulator for drainage (Aker et al., 1998b; Aker et al., 1998a). The drainage simulator was able to simulate successfully the temporal evolution of fluid pressure in three regimes of drainage invasion; viscous fingering, capillary fingering and stable displacement (Lenormand et al., 1988). The presented model is quite detailed and requires substantial computational resources for system sizes above 100×200 lattice points. Therefore very large systems are not accessible. The main change in the presented model is the boundary conditions. Instead of simulating an invasion process, we use biperiodic boundary conditions. The volume of the two fluids are conserved during a simulation. The nature of the simulations is so that after a time the system reaches a steady-state from which intrinsic properties of the system can be found. This gives information on how the fluid is distributed within pore space and the flow properties, *e.g.* the fractional flow. The closest experimental study is that of Avraam and Payatakes (1995a, 1995b, 1999). In etched glass networks they observe complex bubble dynamics far from inlets and outlets.

The paper is organized as follows. Sections 2 to 4 describe the model, *i.e.* the geometrical aspects, the flow conditions, and the moving rules for menisci at nodes respectively. This model is based on the model by Aker *et al.* which is reported on in great detail in (Aker et al., 1998b). We will repeat only briefly the aspects of the model that are unchanged,

and provide details where we have made changes. Finally in section 5 we provide simulation results, and section 6 contains some concluding remarks.

2. The Representation of the Porous Medium and the Geometry of the Fluid Interfaces

The network model presented here is based on the one presented thoroughly in Aker *et al.* (1998b, 1998a). We will refer to that as the *mother model*. The porous medium geometry, and the possible fluid interface configurations are essentially unchanged so only a short resume is given here.

The porous medium is represented by a square lattice of cylindrical tubes, tilted 45° with respect to the overall flow direction. The volume of throats and pores is contained in the tubes. The points where four tubes meet are referred to as nodes. Randomness is incorporated in the system by allowing the position of each node to be randomly chosen within the interval plus minus thirty percent of the lattice constant away from its respective lattice point. The choice of thirty percent is somewhat arbitrary but seems reasonable. From these positions the distance d_{ij} between connected nodes i and j is calculated for all i and j . Further the average radius of the tubes are chosen by random in the interval $(0.1d, 0.1d + 0.3d_{ij})$, where d is the average distance between nodes, *i.e.* the lattice constant. This means that there is a minimum radius assuring that no tubes are effectively blocked. Further the maximum radius is related to the length of the tubes in such a way that short tubes cannot be unreasonably wide. The question of the importance of the topology is addressed in the discussion in section 6.

We consider two fluids within this system of tubes. They are separated by a set of interfaces, menisci, in the tubes. We do not allow for film flow. Motion of the fluid during a simulation is represented by the motion of the menisci. In each tube we allow zero, one or two menisci. If at any instant the evolution of the system, as will be described in subsequent sections, generate a third meniscus in one tube then the three menisci are collapsed into one. The position of this new meniscus is the one which preserves the volumes of the two fluids. This upper limit of two menisci in each tube sets the resolution of the fluid distribution.

With respect to permeability the tubes are treated as cylindrical, but with respect to capillary pressure they are hour-glass shaped. This means that over each of the menisci in the system there is a capillary

pressure which varies with the menisci's positions in the tubes. The formula for the capillary pressure is

$$p_c = \frac{2\gamma}{r}(1 - \cos(2\pi x)) \quad (1)$$

which is a modified form of the Young-Laplace law. r is the radius of the tube, and γ is the inter-facial tension between the fluids. Further, x is a position variable which runs between zero and one. This functional form is mapped onto the central 80 percent of each tube. The closest 10 percent to the nodes is a zero capillary pressure zone, the major purpose of which is to enhance the numerical performance of the model.

3. Flow Conditions and Boundary Conditions

Before we turn to the discussion of the globally applied pressure and the boundary conditions, we consider the flow equation for a single tube. The volume flux through one single tube is given by the Washburn equation for capillary flow (Washburn, 1921);

$$q = -\frac{k}{\mu_{\text{eff}}} \cdot \frac{\pi r^2}{d} (\Delta p - p_c). \quad (2)$$

The tubes are considered as cylindrical with radius r . The fraction $\pi r^2/d$ is the cross-sectional area divided by the length of the tube. The permeability of the tube $k = r^2/8$ as is known from Hagen-Poiseulle flow. When two fluids are present in a tube, an effective viscosity μ_{eff} is used. The viscosities of the two fluids are weighted according to their volume fraction at the beginning of the time step to give μ_{eff} . Further, the pressure p is a discretized field variable with a value in each node. The flow in a tube is proportional to the difference in pressure Δp between the nodes at the ends of the tube. In addition the sum of capillary pressures p_c of the menisci in the tube is subtracted from the pressure difference to give Equation (2) (Washburn, 1921).

The traditional use of network simulators has been the study of invasion processes. Usually the first row of nodes is an inlet row where all the nodes have the same fixed pressure. Similarly the last row works as an outlet row, typically having all nodes fixed at zero pressure. The point being that for a given time step the pressures in these two rows are fixed constraints. The pressures in all the other nodes are free variables that are solved for. The equation that one needs to solve is the conservation of fluid flux passing through each node. This is nothing else than a discrete Poisson problem for pressure.

Once the pressure field is known, Equation (2) gives the flux in each tube. Many authors have studied invasion under a constant applied pressure. The mother model has been used to study constant flux invasion. By solving the flow field for two different globally applied pressures giving two different fluxes, one can calculate the pressure that would give the desired flux. How to do this in practice is described in detail by Aker et al. (1998b). We will just remark for now that all simulations presented in this paper are done with constant flux rate.

Computer power is limited, and in general a detailed model implies small networks and large networks imply coarse models. Our model aims at resolving the dynamics due to variable capillary pressure when passing through throats. It also aims at having a realistic distribution of the two fluids within the pore space as this have consequences for the transport properties of the system. Roughly a system of 100×200 nodes is the maximum size available for simulations with our model within reasonable time. When many data points are needed to probe through parameter space, 40×80 nodes is more realistic.

Invasion simulations go on until the invading fluid reaches the outlet. If they were to go on further, they change character since one fluid is percolating the system. We wish to address the question of what happens in a system far from inlets and outlets, *i.e.* given a very large system, we take out a small piece somewhere in the middle and study its properties.

This is done by adjoining the inlet row and outlet row so that the fluid that flows out of the last row enters the first row. In practice this works in such a way that the simulation can go on for ever, regardless whether one fluid percolates the system or not. In a sense having biperiodic boundary conditions makes the system infinite. However, the system is closed, and there is a fixed volume of each of the fluids in the system. Thus each simulation takes place at constant saturation equal to the one of the starting configuration. We return to this point when presenting results from simulations in section 5.

The straightforward appliance of a global pressure between the inlet row and the outlet row in invasion simulations needs modification. One could do this by adding one row of ghost nodes on both sides of the system. The pressure would be fixed on these two rows as before. The equations would be solved as before, only with the additional constraint that the outgoing flux in each tube between the last row and its ghost row should equal the incoming flux in the respective tube between the other ghost row and the first row. This method works, but has two drawbacks. One is that it gives more complicated computer code. The other is the fact that the pressure is still fixed to have the same value along a straight line through the system, thus giving a boundary effect.

Therefore instead of using ghost nodes with fixed pressures as the driving force we make a jump in the pressure over all the tubes on the boundary. This has been implemented in random resistor networks(Roux, unpublished; Batrouni and Hansen, 1998). It works so that whenever looking across the boundary from one side one sees a positive pressure jump. Whenever looking from the other side one sees a negative jump. The value of the jump is the same in all tubes along the boundary, and will be referred to as the global pressure. The global pressure is the driving force making the fluid go around the system. In order to visualize these boundary conditions one can think of the network as placed on the surface of a torus. The flow is around the torus, but one cannot see any trace of the adjoint boundary. That is the advantage of the pressure jump technique. Otherwise the two techniques give similar results.

4. Updating the Menisci

In the model the entire volume of the porous medium is contained within the tubes. Further, all interfaces between the two liquids are also situated within the tubes. When the fluids flow, all interfaces move according to the flow field. This is straightforward within a single tube. In nodes, however, one needs to define a set of moving rules based on physical reasoning. We also provide an algorithm, which purpose is to generate more realistic motion of two menisci when they are simultaneously approaching the same node.

4.1. UPDATING THE MENISCI WITHIN THE TUBES

The solution of the flow equations provides information on the flux at each instant in every tube. Knowing the cross-sectional area of every tube, we calculate the velocity in every tube from the fluxes. The evolution in time is simply given by explicit Euler integration; every meniscus is moved a distance equal to the velocity in the respective tube, at the beginning of the time step, multiplied by the time step. The time step is chosen so that no meniscus should move a longer distance than, say, ten percent of a tube length. Most of the menisci will remain within the bounds of the tubes after the time step. Some of the menisci have been moved out of the tubes and must be dealt with.

4.2. MOVING THE MENISCI ACROSS THE NODES

The procedure of moving menisci across nodes needs some elaboration. In the mother model(Aker et al., 1998b) this was done in a way which

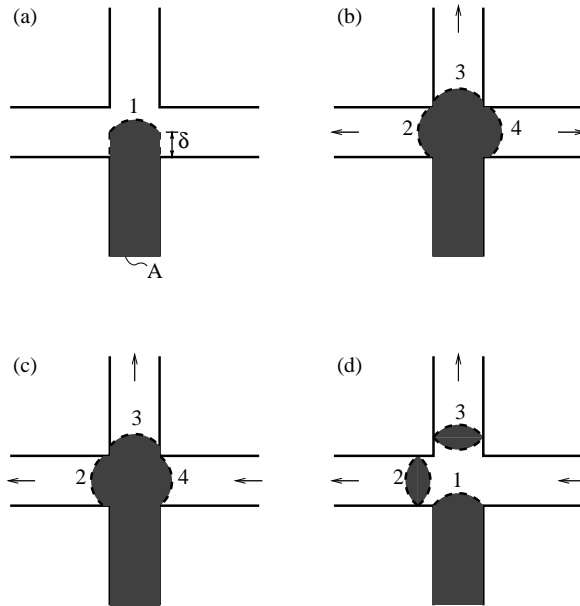


Figure 1. (a) The shaded fluid is entering the node from one tube. The meniscus no. 1 is moved a distance δ into the node, which corresponds to an incoming volume; δA . (b) The case of three tubes carrying outgoing flux. The arrows indicate the flow direction. (c) The case of two tubes carrying outgoing flux. Note that in this case the meniscus no. 4 is left at the edge of the right tube. (d) As (c) one time step later.

was not conserving the volumes of the fluids. This was not a problem in the mother model as the cumulative volume loss over the relevant time scales was small. However, in the present case the model is run considerably longer, and whence these volume losses are no longer acceptable. Also, when simulating an invasion process these small volume changes are easy to come around with the following trick. The invading fluid is coming from an inlet row and the defending fluid is running out on the outlet row, both at a constant flow rate. A change in volume is therefore in such a system equal to a change in elapsed time.

We want to simulate a closed system with fixed saturation, *i.e.* having volume conservation. The strategy is to look at each node and find the menisci which has passed the boundaries of the tubes and are actually ‘moved into’ the node. In the simplest case only one meniscus is inside the node as shown in figure 1(a). The meniscus has been moved a distance δ into the node. This distance times the cross-sectional area of the tube is equal to an amount of volume, $V = A\delta$, which must be moved over to the neighboring tubes. Again in the easiest case the fluid in all three neighboring tubes is flowing away from the node. Then we simply state that we should create one meniscus in each of the three

tubes. They should be placed at distances from the node so that i) the three volumes add up to the one having flown into the node, and ii) the ratios between these three volumes are the same as the ratios between the fluxes in the same three tubes. We illustrate this case in figure 1(b).

This rule does not hold in the case when in one, or more, of the other tubes the fluid flows towards the node instead away from the node. Since we consider immiscible flow we cannot allow the fluids to mix, though somehow that would be the natural idea when two different fluids meet in a node. Within a single time step we allow for a small ‘error’. We place a meniscus on the edge of the tube in which the fluid flow is towards the node. See figure 1(c). The menisci in the other two tubes are placed according to the same principles as before, only now applied to two tubes instead of three. Physically this is equivalent to saying that all of the white fluid coming from the right on the figure pass the node before the shaded fluid enters the node. The roles of the fluids change in the next time step giving the situation shown in figure 1(d). We observe how bubbles have been created in the two tubes carrying outgoing flux. This is an effective mixing of the fluids. This mechanism is the same as in the mother model, and we refer to the discussion there.

These rules generalize quite straightforward to the other possible cases where two or more menisci have entered the node within the same time step. Consider the situation in figure 2(a). The two menisci here situated within the node represent two volumes that have flown into the node. We add the volumes together

$$V_{in} = A_1\delta_1 + A_2\delta_2. \quad (3)$$

Menisci are created in the other two tubes according to the same principles as before. See figure 2(b). This ensures volume conservation,

$$V_{in} = V_{out} = A_3\delta_3 + A_4\delta_4. \quad (4)$$

Also here it may happen that the fluid flow in one tube is towards the node. This is treated in the same manner as before, implying that the last tube will carry all the outgoing flux. These rules works very well. The only scenario not described so far is in the case of having very small bubbles in a tube. During a time step both of the menisci enclosing the bubble may be moved into the node. This is not as tricky as it sounds. One simply has to split the moving job into two parts. First one ignores the second meniscus, or menisci if bubbles are coming from more than one tube, and update everything as before. Then one repeats the procedure considering the second meniscus or menisci according to exactly the same rules.

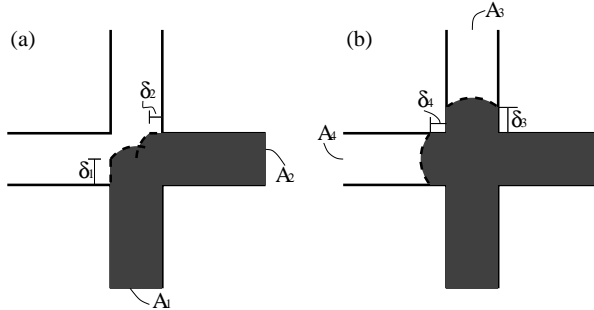


Figure 2. (a) Two menisci are moved into the node in the same time step. (b) Two tubes carrying outgoing flux. The menisci positions δ_3 and δ_4 are chosen so that outgoing volume is equal to incoming volume, and so that the ratio δ_3/δ_4 is equal to the flux ratio in the two tubes.

We remark here that when two menisci enter the node within the same time step they are joined together in the sense that no bubbles are created. If they were to arrive to the node closely after each other bubbles of the withdrawing liquid will remain in the tubes. Consequences of this will be addressed in the next subsection.

4.3. IMITATING THE MERGING OF MENISCI IN THE NODES

In our time integration we need to choose a time step. We do not have a fixed time step, but choose one that does not move any meniscus more than a certain fraction of the tube length. The velocity field in the network will contain local velocities that differs by several orders of magnitude due to geometrical heterogeneity of the network or due to the current fluid configuration. Local velocities and the choice of time step together implies that sometimes or some places two menisci approaching the same node will arrive at the node within the same time step. In other cases it will not. We illustrate this situation in figure 3(a). Here we see that the two menisci in figure 3(a) could reach the node in the same time step which gives the evolution shown in the figures 3(b) and 3(c). If the time step is shorter so that only one of the menisci reaches the node during the time step, the situation will be like in the figures 3(d) and 3(e).

The time step is often recognized as one of the parameters of a dynamical system. The fact that the exact evolution of the system will depend on the choice of time step is unavoidable. It does not really matter as it is the statistical properties that we seek, and they should not change. However, a large time step will in general allow for many pairs of menisci to meet in the node during the time step, and whence be joined together. A small time step will in general make one of the

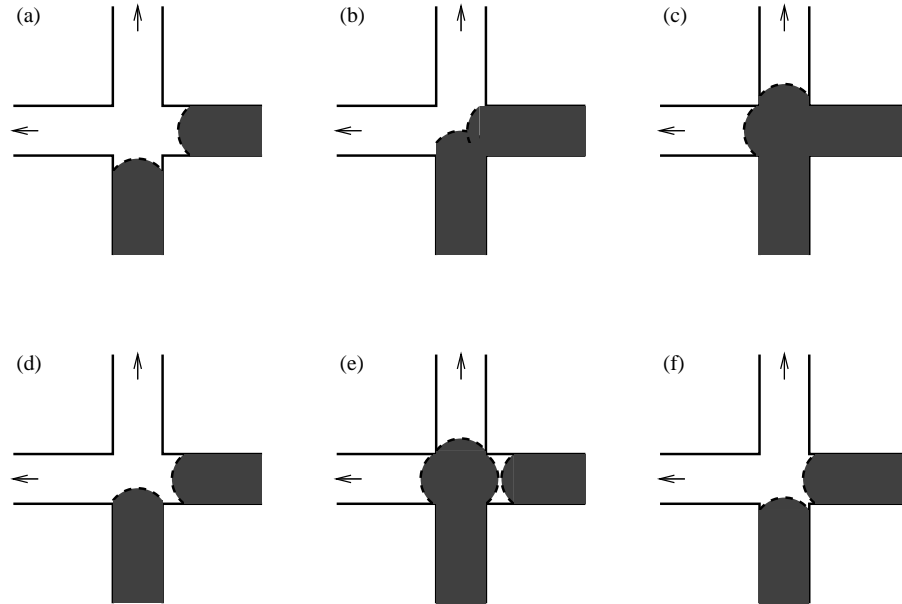


Figure 3. The detailed evolution around a node is dependent on the size of the time step. (a) Two menisci are approaching the same node from neighbouring tubes. (b)-(c) The time step is just long enough such that both menisci enter the node within the time step. The menisci are merged - there are no bubbles created. (d)-(e) The time step is a little shorter and only one meniscus enters the node. A bubble is formed in the tube to the right, and the menisci are not allowed to join. (f) Adjustment of the two menisci in (d) such that they will both enter the node in the next time step.

menisci arrive earlier than the other in the otherwise same situations. These menisci are then not joined together. This time step dependency is clearly unphysical, and we wish to reduce it as much as possible.

This procedure is actually quite important because we know that an actual porous medium has volume in its pores. It takes some time to fill a pore, and menisci will not just pop over to the other side instantaneously. Here there is a difference between a drainage step and an imbibition step. In drainage when a meniscus passes through the threshold of a throat entering into the pore, there has been a local pressure buildup giving rise to a small burst (Haines, 1930; Lenormand and Zarcone, 1983; Måløy et al., 1992). The pressure buildup and subsequent release make the flow into the pore quite fast, and the time to fill the pore quite short. In imbibition the capillary forces make the pores the hardest areas to pass, meaning that wetting fluid needs more time to fill up the volume of the pores.

In our model menisci are moved instantaneously across pores. This is unphysical. If the physical situation is that two menisci enter into

the pore volume at the same time, then some kind of mixture is likely to happen. Bubbles can be created or the menisci can join together pushing the other liquid out on the other side first. The circular disk model successfully studied by Cieplak and Robbins (1990) provides some basic intuition on this problem. We are dealing with a situation that is neither wetting nor nonwetting invasion globally due to the biperiodic topology of the network. Locally both wetting and nonwetting invasion steps happen all the time. The detailed knowledge about how menisci advance through pore volumes (Cieplak and Robbins, 1990) is too complicated to be incorporated fully in our model.

Instead our model aims at grasping the bare cut essence of adjoining menisci in pores. First we associate an effective volume to each node. Since the node is the meeting point of four tubes, it is reasonable to assume that the volume in the end of each tube add up to an effective node volume. We have chosen to say that 20% of each tube volume is added to the respective pore volumes. The curvature of the tube when modeling capillary pressure starts at a distance that is ten percent of the tube length away from the node. 20% is roughly where the tubes start to get narrow.

Thus, having assigned an effective volume to every node, we can estimate the time needed to fill the nodes whenever a meniscus has entered into a node. According to the position of the meniscus in the node we know how much volume that is already in the node. Here one should include the 20% end part of the tube from which the meniscus arrived. Knowing the instantaneous flux in the tube from which the meniscus came, we can calculate an estimate for the filling time by taking the remaining volume and divide it by the flux. Further, since we know the velocities in the other tubes, we can for every meniscus that is moving towards the node calculate an estimate for the arrival time to the node for the menisci. If this arrival time for one other meniscus is shorter than the filling time for the one that has arrived to the node, one can say that physically these two menisci should have been present in the node at the same time.

So, if that happens we assume that the menisci physically would have joined together. In our model being joined together is equivalent to arrive into the node in the same time step. Therefore the time evolution is organized as follows. First all menisci are moved after the naive Euler scheme. Then for every node we check if there is one single meniscus inside it. If it is, we calculate its filling time and find the shortest arrival time for any other meniscus to that node. If these times show that the menisci should physically have met in the node, we move both menisci so that they are equally distant from the node, see Figure 3(f). This is done under the constraint of volume conservation. Then it might

happen that after this movement both menisci are inside the node or they are both outside the node. In either case the procedure has now come to moving the menisci which are still inside the nodes. This is done as described in detail in the previous subsection. Eventually the flow equations are solved anew for the new fluid configuration and the whole process is repeated.

In this subsection we have described how we simulate merging of menisci in nodes. The mother model did not have this feature, but it was used to study drainage invasion processes. In an invasion process the number of menisci arriving at a node approximately at the same time, and whence being subject to this routine, is quite small. Here we have biperiodic boundary conditions allowing for simulations to go on for a much longer period of time. In particular it allows the system to reach fully developed flow far from initial fronts and configurations. Fully developed two-phase flow is reported on in Avraam and Payatakes (1995a, 1995b, 1999), where the number of bubbles or clusters of the fluids is large. Therefore it is important to take into account not only the possibility of breaking up bubbles, which happens whenever passing through a node, but also this mechanism of merging bubbles based upon physical reasoning.

In practice during a simulation this routine make adjustments so that both nonwetting pairs of menisci and wetting pairs of menisci are joined. However this happens more often in the wetting case. The routine has a larger effect of making the wetting phase more compact than is the case for the nonwetting fluid. This is in agreement with the well-known fact that considerable smoothing of the invasion front takes place in wetting invasion (Lenormand and Zarcone, 1983; Cieplak and Robbins, 1990).

5. Simulations

We will in this section provide simulation results. The general nature of the simulations will be addressed in the first subsection. Thereafter we discuss the relevance and importance of possible parameters of the system. They include viscosities, interfacial tension, flow rate, and system size. Finally, detailed results are given for the case of two fluids with equal viscosity using the capillary number as parameter.

5.1. THE NATURE OF THE SIMULATIONS

We start out by giving data samples from two simulations before turning to generalities. The system is 20×40 nodes in both simulations.

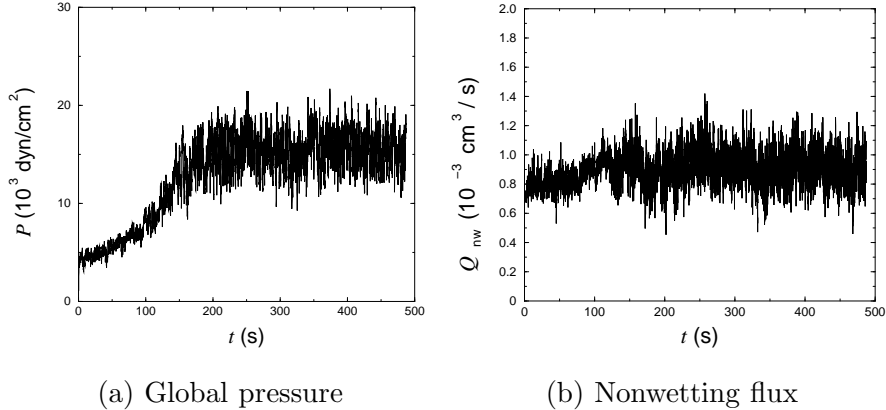


Figure 4. Typical time evolution of a simulation. Here the nonwetting saturation is about 52% and the capillary number is $C_a = 3.2 \times 10^{-4}$. The fluid travels on the average approximately twice around the system during this simulation.

The initial configuration of the systems is one horizontal region with wetting fluid and another with nonwetting fluid. In the first sample the nonwetting volume fraction, *i.e.* the saturation is 52%. In the second case it is 42%.

Both fluids have the same viscosity; $\mu = 1.0$ P. The interfacial tension between the fluids is $\gamma = 30.0$ dyn/cm. The flow rates are respectively $Q_{\text{tot}} = 1.38 \times 10^{-3}$ cm³/s and $Q_{\text{tot}} = 1.38 \times 10^{-2}$ cm³/s. The capillary number is defined as follows

$$C_a = \frac{\mu Q_{\text{tot}}}{\gamma \Sigma}, \quad (5)$$

where Σ is the cross-sectional area of the network. Physically the capillary number is the ratio between viscous and capillary forces. Our two cases have $C_a = 3.2 \times 10^{-4}$ and $C_a = 3.2 \times 10^{-3}$.

The total flux Q_{tot} is equal to the sum of the wetting flux and the nonwetting flux. During the simulations the total flux is held at a fixed value. However, it is the physics of the systems that determine the flux of the wetting and of the nonwetting fluids respectively. Fluid motion means reorganization of menisci and capillary forces change. In general when the viscosities of the fluids are different, the effective viscosity of the fluid in each tube also change along with the time evolution. In order to keep the total flow rate constant, the globally applied pressure must be adjusted in every time step.

The results from the two samples are shown in the figures 4 and 5. They show the global pressure and the nonwetting flux versus time. The curves are noisy on the time scale used in these plots. One should note that the time axis is compressed so that the data points are close.

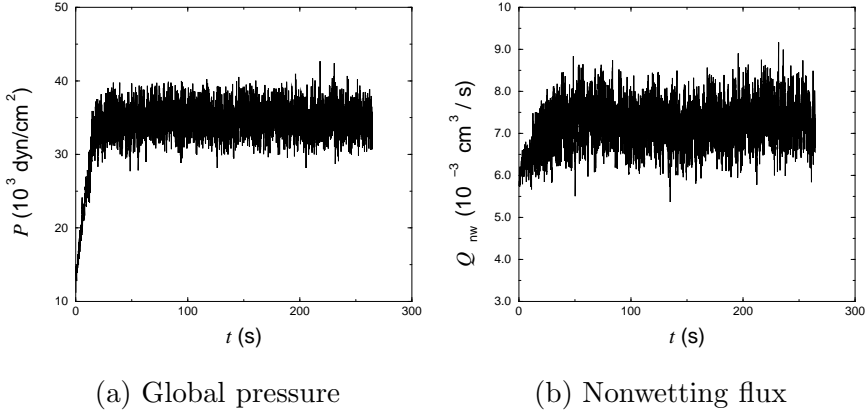


Figure 5. Typical time evolution of a simulation. Here the nonwetting saturation is about 42% and the capillary number is $C_a = 3.2 \times 10^{-3}$. The fluid travels on the average approximately eight times around the system during this simulation.

What looks like a jump on the plot may very well be 20 or 100 time steps in the simulation.

The curves for the global pressure are very characteristic. There is a transient part and a steady part. This means that at the beginning of a simulation the system remembers its initial configuration. After some time which depends on system parameters, the system reaches a steady-state. In figure 4(a) the capillary number is a factor ten smaller than in figure 5(a). We can see how this makes the transient period longer in the first case.

We are not really interested in the transient part. The important aspect is that the systems reach a steady-state. In this state all fluid is mobilised. We know this by looking at consecutive images of the fluid distribution. This means that the steady-state is characteristic of the medium and the fluids; the state will be reached whatever initial configuration. We will return to possible history dependence for other capillary numbers than depicted here in the next subsection.

Figures 4(b) and 5(b) show the nonwetting flux averaged over the entire system as a function of time. The curves are not normalized with respect to total flux. We merely wish to show their character. Their transient parts are not so explicitly distinct from their steady parts as is the case for the global pressure evolution in these samples. In general we have used both curves to determine a time after which the systems for sure have reached the steady-state. When the system has reached the steady-state we have found the time average of the global pressure, the wetting flux Q_w and the nonwetting Q_{nw} flux. Since the simulations have gone on for in the order of 50000 time steps after reaching this

state, the statistics are good. We focus the rest of the presentation of results on one of the more interesting property of the systems. That is the fractional flow of one of the fluids as a function of the system parameters.

5.2. RELEVANT PARAMETERS

One important parameter of the system in these simulations is the nonwetting saturation S_{nw} , which is the volume fraction of the nonwetting fluid. The corresponding output is the fractional flow of the nonwetting fluid

$$F_{\text{nw}} = \frac{Q_{\text{nw}}}{Q_{\text{tot}}}. \quad (6)$$

Figures 6 and 7 show how the nonwetting fractional flow is a function of the nonwetting saturation. The S-shape is resemblant of the one found in Buckley-Leverett fractional flow (Dullien, 1992). Both figures show the curves obtained for $C_a = 1.0 \times 10^{-3}$. The shapes and their dependency of C_a will be discussed in the next subsection.

We have done simulations for fluids with equal viscosity. The interfacial tension has been $\gamma = 30.0 \text{ dyn/cm}$ for all simulations. The total flux have been changed from simulation to simulation in order to give the desired capillary number after Equation (5). We wish to demonstrate that for the case of equal viscosities then the capillary number is the relevant parameter for the fractional flow curves.

From Equation (5) we see that the capillary number is unchanged if Q_{tot} and γ are scaled with the same factor. If γ is scaled with a factor, so is all capillary pressures after Equation (1). When the scaled p_c is inserted into Equation (2) one can simply choose to scale Δp and q with the same factor. Cancellation of the factor on both sides of the equation shows that this is the solution of the problem when also the total flux is scaled with this factor. This argument assures that the interfacial tension between the fluids can be chosen to a reasonable value in the simulations. The dependence on the capillary number will be the same.

Keeping the surface tension γ fixed, and thus p_c from Equation (1) fixed, this way of reasoning can be used also on the relationship between the viscosity and the total flux. They appear as the product μQ_{tot} in Equation (5). As long as both fluids have the same viscosity then the effective viscosity μ_{eff} in Equation (2) is equal to the same μ for all tubes. If on the other hand the fluids have different viscosity then the effective viscosity will in principle change independently in each tube. So for equal viscosities a change in the viscosity and an inverse change in the flux q will cancel out, in Equation (2), like in the case for the interfacial tension. Figure 6 shows this effect. Here

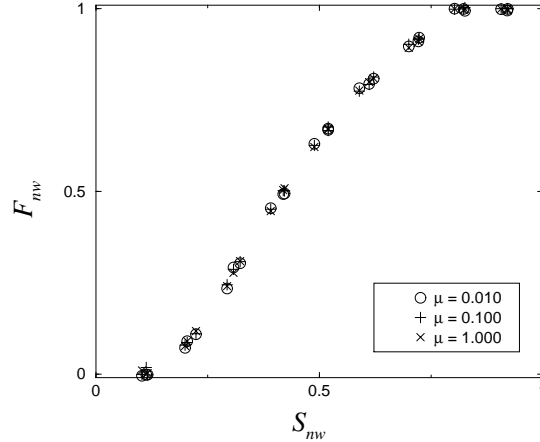


Figure 6. The nonwetting fractional flow versus the nonwetting saturation for capillary number $C_a = 1.0 \times 10^{-3}$. The system size is 20×40 . The viscosity of both fluids have been given the same three different values. We observe the data-collapse which is expected.

the capillary number is fixed at the value $C_a = 1.0 \times 10^{-3}$ while the viscosity is allowed three different values. The system size is 20×40 nodes and three different random seeds giving three different geometries are used. The saturation have been varied between 10% percent and 90%, roughly. The data-collapse is very good as it should be. Three and three data points should according to our reasoning be equal. However, round-off makes the exact evolution of the system different for each viscosity used. Therefore the points will not be identical. The small differences can be considered as a measure of the error bars of the time averaging process.

The last parameter to examine in Equation (5) is the cross-sectional area Σ . The number of nodes L_x in the cross-section is proportional to the cross-sectional area. Further the number of rows of nodes L_y is also a possible parameter of the curve, even though not included into the expression (5). Figure 7 shows the result for two different system sizes; $L_x \times L_y = 20 \times 40$ and $L_x \times L_y = 40 \times 80$. The capillary number is fixed at the same value as in Figure 6. We see that the curves collapse onto each-other. This is a non-trivial result. Typically invasion simulations give scaling relations between, *e.g.* the front width, and the system size. Here we find that the results are size independent. In figure 7 both L_x and L_y are changed at the same time. One could imagine that there were an individual dependence on each of them that cancels out. We have checked this, and there is not. The size independence must be understood as a result of the construction of the system. The system

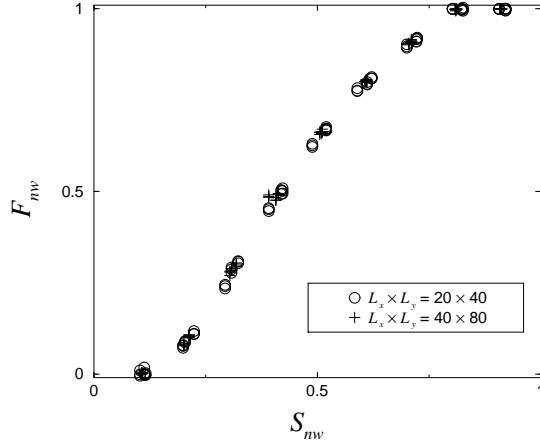


Figure 7. The nonwetting fractional flow versus the nonwetting saturation. Two different system sizes, 20×40 and 40×80 , have been used in the simulations. This data collapse show the size independent nature of the simulations.

is forced to have a certain saturation. It is reasonable to think that saturation heterogeneities are only visible below a certain length scale, in terms of number of nodes, within the system. Above this length scale the system has homogeneous saturation. Each system or part of the system above this scale should display the same properties, and that is what we see.

5.3. FRACTIONAL FLOW CURVES

In the previous subsection we found out that for two fluids having equal viscosity the capillary number serves as the relevant parameter for fractional flow versus saturation curves. Figure 8 shows the obtained curves for six different capillary numbers. In (a) to (e) data points for both system sizes 20×40 and 40×80 are plotted on top of each-other. The data in (f) are only from the smaller system size, and the result is more tentative due to possible history dependency.

The lower the capillary number, the larger a role play the capillary forces. Capillary forces may be sufficiently strong to hold bubbles of one fluid fixed in one place. However, for large capillary numbers all fluid is mobilised. This means that the memory of the system is very short. After a while all relics of the initial fluid distribution is gone. We will make a subdivision of parameter space into history independent and history dependent. The figures 8(a)-(e) is in the history independent regime. By visual inspection we have observed that for the capillary number $C_a = 1.0 \times 10^{-4}$ pieces of the initial configuration can be seen all the time during the simulations. This also happens whenever the final

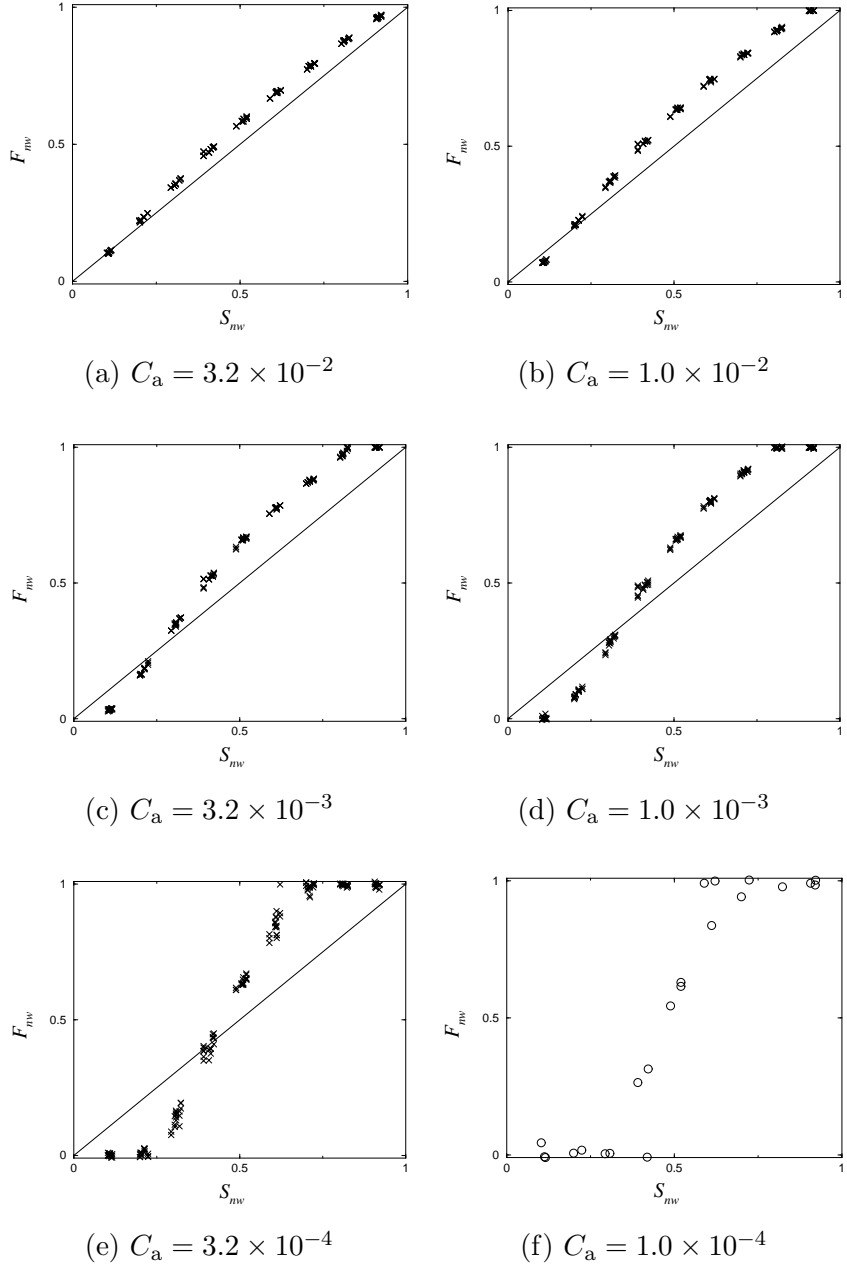


Figure 8. The plots show the nonwetting fractional flow versus the nonwetting saturation for the case of two fluids having equal viscosity. The capillary number is the parameter. (a)-(e) are in the history independent regime, while (f) is in the history dependent regime and is thus more tentative.

situation is one where one fluid percolates and flows, while the other is immobile. If this were the final situation whatever initial configuration then it would not indicate history dependence. However, in the plot 8(f) we can see how different results almost the same saturation (at 40% and at 60%) can give. It is in the history dependent regime. Here we also needed to simulate for a longer period of time to reach the steady-state. Further, general analysis of history dependent systems should be done with more care than we have done here, taking into account at least a number of possible initial configurations. Therefore we classify this plot as tentative.

In the plots in figure 8 a diagonal line is added. This is the line where the nonwetting fractional flow is equal to the nonwetting saturation. It is interesting to use this line as a reference and note how the data points lie above or below this line. Looking at the five plots 8(a)-(e) in the history independent regime, we can say that (a) and (b) share the property that almost all data points are above the diagonal. In (d) and (e) the curves are S-shaped, while (c) makes an intermediate situation.

The plots (a) and (b) can be said to be in a viscous force-dominated regime. We can very well classify the history dependent regime as a capillary force-dominated regime. The regime in-between, plots (d) and (e), constitutes a viscous and capillary interactive regime.

In the viscous force-dominated regime the fractional flow curves are close to the diagonal. Had there been no capillary forces, no wetting difference, the fluids would have been interchangeable. This symmetry would have implied the fractional flow curve to be the straight line. However, there are capillary forces which statistically will make the wetting fluid occupy narrower tubes more frequently than is the case for the nonwetting fluid. Since the flow is faster in wider tubes, the fractional flow of nonwetting fluid is larger than the nonwetting saturation in this regime.

The interaction regime is more complex. The main aspect here are the distribution of the two fluids within pore space and the velocity field. For large nonwetting saturations the nonwetting fractional flow is larger than the saturation, and for small nonwetting saturation the fractional flow is smaller. Whenever one can find pathways through the network that contain few interfaces, they will in general carry more flux. There is a fundamental asymmetry in that the wetting fluid prefers being within tubes while nonwetting fluid prefers being situated around nodes. This implies that the fluid distribution is asymmetric. Our simulations show that larger compact wetting regions occur. Nonwetting structures are more branched, treelike, surrounding the wetting areas, generally speaking. A large wetting saturation implies that the pathway of least resistance passes through the compact wetting regions. Likewise

for large nonwetting saturations the pathway is along the nonwetting branches. Briefly this explains qualitatively the S-shape of the curves in this regime.

The methodology is the main point of this article. Further discussions about fluid distribution and velocity or flux distributions could eventually provide additional insight but will be studied elsewhere. The main result is the S-shaped curves which bear a strong resemblance with the one obtained by Buckley and Leverett. Much work has been done in calculating fractional flow curves from conservation principles using differential equations (Binning and Celia, 1998). The present result should be considered placed within that picture. Our network simulator provides a fundamentally different approach to the problem. Without going into any detailed comparison one can say that the results are similar. In our simulations the S-shaped curve is shifted to left. This asymmetry is due to the capillary forces. This possibility to include capillary forces is one of the major advantages of the simulation method.

6. Concluding Remarks

We have presented a two-dimensional network simulator for two-phase flow. The model is based on a model which successfully has simulated drainage invasion (Aker et al., 1998b). The major change is the introduction of biperiodic boundary conditions. This makes the system closed in the sense that the volume of the fluids is conserved. The system is studied under a constant flux in one direction. This is done by explicit Euler time integration, and in each time step the appropriate global pressure, that gives the desired flux, is used. By this method we have investigated the fractional flow properties of the system as a function of various parameters. These include the viscosities of the fluids, the total flux rate and the network size. The viscosity ratio and the capillary number are the important effective parameters.

We have studied the case where the two fluids have equal viscosity, varying the capillary number. In particular we found that for a fixed capillary number, the results were independent of the system size. The fact that fractional flow curves can be obtained by this method, simulating on reasonably small system sizes, makes it possible to obtain useful information with present computer power. Many questions need further investigation, the effect of changing the viscosity ratio being the most prominent.

The possible dependence on topology is also a question that one should consider. General knowledge from percolation theory indicates

that the choice of a square network as opposed to other regular networks should not make much difference (Stauffer and Aharony, 1992). However, there is *in principle* no problem to expand the model to a irregular set of nodes, having an irregular connectivity. The qualitative knowledge should not change significantly by doing this. However, if one wish results that are valid for a specific medium, higher quantitative precision may be desirable and obtainable in this way.

Based on the results presented here we divided parameter space into a division between history dependent and history independent regime. The method works very well in the history independent regime. Whenever history dependence is important, care should be taken not ignore possible impact of history on final results. Further a division of the history independent regime was made into a viscous force-dominated regime and a viscous and capillary interactive regime. The latter being the more interesting having S-shaped fractional flow curves. These curves are comparable to the Buckley-Leverett type fractional flow curves. The simulator presented here constitutes a different approach to obtaining this kind of data.

Acknowledgements

H.A.K, E.A. and A.H. thank the Niels Bohr Institute and Nordita for friendly hospitality and support. H.A.K. acknowledges support from VISTA, a collaboration between Statoil and The Norwegian Acad. of Science and Letters. E.A. acknowledges partial support from NFR through a SUP grant. We also like to thank Knut Jørgen Måløy for valuable comments.

References

Aker, E., K. J. Måløy, and A. Hansen: 1998a, 'Simulating temporal evolution of pressure in two-phase flow in porous media'. *Phys. Rev. E* **58**, 2217–2226.

Aker, E., K. J. Måløy, A. Hansen, and G. G. Batrouni: 1998b, 'A Two-Dimensional Network Simulator for Two-Phase Flow in Porous Media'. *Transport in Porous Media* **32**, 163–186.

Avraam, D. G. and A. C. Payatakes: 1995a, 'Flow regimes and relative permeabilities during steady-state two-phase flow in porous media'. *J. Fluid Mech.* **293**, 207–236.

Avraam, D. G. and A. C. Payatakes: 1995b, 'Generalized Relative Permeability Coefficients during Steady-State Two-Phase Flow in Porous Media, and Correlation with the Flow Mechanisms'. *Transport in Porous Media* **20**, 135–168.

Avraam, D. G. and A. C. Payatakes: 1999, 'Flow Mechanisms, Relative Permeabilities, and Coupling Effects in Steady-State Two-Phase Flow through Porous Media. The Case of Strong Wettability'. *Ind. Eng. Chem. Res.* **38**, 778–786.

Batrouni, G. G. and A. Hansen: 1998, 'Fracture in Three-Dimensional Fuse Networks'. *Phys. Rev. Lett.* **80**, 325–328.

Binning, P. and M. A. Celia: 1998, 'Practical implementation of the fractional flow approach to multi-phase flow simulation'. *Advances in Water Resources* **22**, 461–478. and references herein.

Blunt, M. and P. King: 1990, 'Macroscopic parameters from simulations of pore scale flow'. *Phys. Rev. A* **42**, 4780–4787.

Buckley, S. E. and M. C. Leverett: 1942. *Trans. Am. Inst. Min. Eng.* **146**, 107.

Chen, J.-D. and D. Wilkinson: 1985, 'Pore-scale viscous fingering in porous media'. *Phys. Rev. Lett.* **55**, 1892–1895.

Cieplak, M. and M. O. Robbins: 1990, 'Influence of contact angle on quasistatic fluid invasion of porous media'. *Phys. Rev. B* **41**, 11508–11521.

Dullien, F. A. L.: 1992, *Porous Media: Fluid Transport and Pore Structure*. Academic Press, San Diego.

Haines, W. B.: 1930, 'Studies in the physical properties of soil'. *J. Agr. Sci.* **20**, 97–116.

Koplik, J. and T. J. Lasseter: 1985, 'Two-phase flow in random network models of porous media'. *SPE J* **2**, 89–100.

Lenormand, R., E. Touboul, and C. Zarcone: 1988, 'Numerical models and experiments on immiscible displacements in porous media'. *J. Fluid Mech.* **189**, 165–187.

Lenormand, R. and C. Zarcone: 1983, 'Mechanism of the displacement of one fluid by another in a network of capillary ducts'. *J. Fluid Mech.* **135**, 337–353.

Måløy, K. J., J. Feder, and T. Jøssang: 1985, 'Viscous fingering fractals in porous media'. *Phys. Rev. Lett.* **55**, 2688–2691.

Måløy, K. J., L. Furuberg, J. Feder, and T. Jøssang: 1992, 'Dynamics of slow drainage in porous media'. *Phys. Rev. Lett.* **68**, 2161–2164.

Paterson, L.: 1984, 'Diffusion-limited aggregation and two-fluid displacements in porous media'. *Phys. Rev. Lett.* **52**, 1621–1624.

Rothman, D. H.: 1990, 'Macroscopic laws for immiscible 2-phase flow in porous media - results from numerical experiments'. *J. Geophys. Res.*

Roux, S.: unpublished.

Stauffer, D. and A. Aharony: 1992, *Introduction to Percolation Theory*. Taylor & Francis, London.

Washburn, E. W.: 1921, 'The dynamics of capillary flow'. *Phys. Rev.* **17**, 273–283.

Wilkinson, D. and J. F. Willemsen: 1983, 'Invasion percolation: A new form of percolation theory'. *J. Phys. A* **16**, 3365–3376.

Witten, T. A. and L. M. Sander: 1981, 'Diffusion-limited aggregation, a kinetic critical phenomenon'. *Phys. Rev. Lett.* **47**, 1400–1403.